J. Jpn. Soc. Powder Powder Metallurgy, **72** (2025) S211-S218
https://doi.org/10.2497/jjspm.14E-T16-02

Field Assisted Sintering in the Direct Recycling of Hot Deformed Nd-Fe-B Magnet Scrap

Monica KESZLER[1]*, Felix GROSSWENDT[2], Anna-Caroline ASSMANN[3], Martin KRENGEL[4], Fernando MACCARI[5], Oliver GUTFLEISCH[5], Doris SEBOLD[1], Sebastian WEBER[2], Olivier GUILLON[1], and Martin BRAM[1,2]

[1]Forschungszentrum Jülich GmbH, Wilhelm-Johnen-Strasse, Jülich 52428, Germany
[2]Ruhr-Universität Bochum, Institut für Werkstoffe, Universitätsstraße 150, 44801 Bochum, Germany
[3]Lehrstuhl für Anthropogene Stoffkreisläufe, RWTH Aachen, Intzestrasse 1, 52072 Aachen, Germany
[4]Wilo SE, Wilopark 1, 44263 Dortmund, Germany
[5]Technische Universität Darmstadt, Institut für Materialwissenschaft, Peter-Grünberg-Straße 2, 64287 Darmstadt, Germany

Abstract
With the expanding use of high-performance permanent magnets, such as Nd-Fe-B, in green energy production and e-mobility, comes the need to further investigate contemporary production methods. Field assisted sintering technologies, such as spark plasma sintering and flash spark plasma sintering, have shown promising results with regards to anisotropic texturing, densification, and microstructural fine-tuning, even from non-ideal crushed anisotropic Nd-Fe-B scrap as a starting powder. Optimization of these processes could lead to magnetic performance that matches or exceeds standard commercial magnet production techniques, such as hot deformation. This is due to the fine parameter monitoring and control available with field assisted sintering devices. This study focuses on the optimization of field assisted sintering with commercial MQU-F to demonstrate net-shaping of anisotropic Nd-Fe-B magnets with an intention of transferring the parameters to the deformation of recycled magnet powder.

Keywords: recycling, permanent magnets, Nd-Fe-B, field assisted sintering, circular economy

Introduction

Permanent magnets play a large role in a wide variety of applications, including wind energy, electric vehicles, and consumer electronics. Currently, the magnets known to have the highest maximum energy product, $(BH)_{max}$, are Nd-Fe-B based magnets, with a theoretical $(BH)_{max}$ of 512 kJ m^{-3} [1–3]. To tune the properties of these magnets, certain elements known as heavy rare earth elements (HREEs) are added. The addition of these REEs lead to changes in properties such as a magnet's temperature tolerance or its coercivity, H_{cJ}, which is the magnet's resistance to demagnetization [4]. These HREEs include Dy and Tb, of which mining is localized to just a few countries such as China, the USA, Australia, and India. With growing interest in green energy production and e-mobility, the demand for REEs and HREEs will continue to be difficult to meet. However, with increased production of electronics including REEs and Nd-Fe-B comes the increase in e-waste streams, from which REEs can be extracted again to be recycled. This could mitigate the supply risk to some degree in the mid-term [5].

There are three primary types of Nd-Fe-B magnets for industrial applications, which are divided according to how they are prepared. These types are sintered magnets, deformed magnets, and polymer-bonded magnets. Both sintered and deformed magnets do not contain any amount of polymer binder and therefore have a higher Nd-Fe-B content than polymer bonded magnets. A higher volume of Nd-Fe-B leads to an exhibition of better magnetic performance. Sintered magnets are produced via Nd-Fe-B microcrystalline powders, which are then magnetically aligned, compacted, and freely sintered [6]. Hot deformed magnets, though, are formed through nanocrystalline powder in a two-stage process, with the first stage consisting of hot pressing and the second stage consisting of either die upsetting or extrusion. The combination of these stages lead to both a fully dense magnet and an anisotropic microstructure [7]. Sintered and hot-deformed magnets have become attractive candidates for recycling for two primary reasons. Firstly, these magnets have high REE content, more than 30 wt%. Secondly, these magnets can maintain their original physical and chemical properties within their bulk even after their use phase, even with deterioration on their surface. Despite this, the recycling focus of these magnets tends towards melting and re-forming rather than direct recycling.

Current direct alloy recycling techniques of interest include melt-spinning, hydrogen-decrepitation-desorption-recombination (HDDR), or recasting into a master alloy [8–10]. If a sintered magnet is crushed and re-sintered into a new magnet, the magnetic performance decreases with each consecutive crushing and reforming. This is likely due to the oxidation of Nd, a primary component of the grain boundary layer. This oxidation both subtracts Nd from the grain boundary phase and hinders the grain boundary from melting during sintering. The primary method of replacing oxidized Nd is adding additional Nd to the sintered magnet powder [11]. Melt-spinning, which requires the melting of Nd-Fe-B and casting onto a molybdenum wheel, produces microstructurally amorphous or

*Corresponding author, E-mail : m.keszler@fz-juelich.de

nanocrystalline flakes. This method unfortunately requires large power consumption due to the necessity of melting the Nd-Fe-B, and it also has a loss of about 20-30 wt% of the magnet material [8,12]. HDDR requires the use of hydrogen and temperature, adding additional steps to the recycling process. Unlike sintered magnets, hot-deformed magnets also have a tailored anisotropic microstructure that would be affected negatively by extensive thermal treatments. When hot-deformed magnets are deformed, the crystal grains are thermomechanically aligned as their aspect ratio is increased, leading to a lateral diameter of roughly 200-500 nm and a thickness of 20-50 nm. Simultaneously, the c-axis of the grains is aligned to the direction of applied force [13,14]. According to Hioki *et al*., a Nd-rich, liquid grain boundary phase acts as lubricant and promotes anisotropic grain growth through grain boundary migration and solution-precipitation creep [13]. Using powder generated from crushed hot-deformed magnets to form a recycled sintered magnet would be a detriment, as thermomechanical grain alignment would not occur and excessive grain growth would decrease H_{cJ} [13,15].

In contrast to the methods listed above, electric current-assisted sintering (ECAS) technologies have been considered in the use of producing anisotropic magnets directly from crushed hot-deformed magnet material. A combination of field assisted sintering techniques/spark plasma sintering (FAST/SPS) and flash SPS have been shown to generate magnets with viable properties from recycled magnet material [16–18]. FAST/SPS is a powder metallurgical technique that requires the use of an electric current flow to generate heat and sinter powder. Using a uniaxial pressure, it can compact magnet powder in a similar fashion to hot compaction. Unlike hot compaction, the use of the electric current for heating allows for high heating rates and direct heating through Joule effects (resistance heating), therefore leading to rapid consolidation [19,20]. A quick heating rate allows for a shorter time for anisotropic powders, like hot-deformed magnet powder, to be kept at high temperatures, reducing grain growth [16,18,21]. Flash SPS behaves as the hot-deformation step. Using a single power pulse and applied uniaxial pressure, a pre-compacted form sintered via FAST/SPS can then be deformed into a fully dense magnet. This method of deformation also initiates c-axis rotation to align with the pressing direction and anisotropic grain growth in commercial magnet powders [16,18]. In recycled hot-deformed magnet powders, the grain rotation phenomenon is not seen so predominantly as in isotropic powders during flash SPS. However, it is possible to consolidate recycled hot-deformed Nd-Fe-B particles into a matrix of commercial isotropic magnet powder without inducing excessive grain growth via flash SPS [17].

This work aims to explain the ongoing optimization of the use of FAST/SPS and flash SPS in the recycling of hot-deformed magnet scrap. The main focus is to demonstrate the ability to produce net-shaped magnets by these technologies. Two methods are demonstrated. Firstly, a boron nitride ring die to further shape flash SPS deformed magnets is utilized. Secondly, FAST/SPS is explored as the hot-deformation step in place of flash SPS. Commercial MQU-F powder was used as starting material for both approaches easing the benchmark with existing results [16–18,22–24]. Transfer to scrap powder from hot-deformed Nd-Fe-B magnets will be the focus of our ongoing work.

Experiment

Starting Powders

All pre-sintering and deformation parameters were tested using Magnequench MQU-F melt-spun powder (batch number B55557), except for one trial with recycled material. This is a commercially available melt-spun Nd-Fe-B powder with a ribbon-like morphology, and it is commonly used as standard material for the production of hot-deformed anisotropic magnets. The ribbons contain nanocrystalline, isotropic grains of roughly 50 nm. The oxygen content of the pristine MQU-F powder batch was 1120 ppm. A variety of studies have used this powder or similar for the demonstration of sintering technologies such as FAST/SPS, flash SPS, and electric discharge sintering (EDS) [14,16,17,22–24]. Utilization of this magnet powder allows for the direct comparison of the effects of the FAST/SPS and flash SPS process between scrap magnet powder to pristine magnet powder.

Previous work involving the ECAS processing of scrap Nd-Fe-B hot-deformed magnets concluded that the ideal particle size of crushed magnets is roughly 125-1000 μm. This is due to smaller particles absorbing more oxygen than their larger counterparts [17,25]. For example, a powder containing particle size fractions <200 μm had an oxygen content of 6000 ppm [17]. For the preliminary experiment shown in this work, scrap Nd-Fe-B crushed to 500-1000 μm was used. This powder had a lower oxygen content at only 2350 ppm. The control of oxygen contamination is important to avoid creating Nd-oxides, which would detract from the available Nd in the system to form the Nd-rich grain boundary phase. Crushing was done in a glove box using a type BB 50 jaw crusher (Retsch GmbH, Haan, Germany) and the resulting powder was sieved to the desired particle size range. Oxygen content within the glovebox was controlled via the pumping of nitrogen into the box during the crushing process. Due to imperfect sealing, a small amount of oxygen enters the chamber from the air resulting in a residual oxygen content of 0.3 vol.%. The recycled stream is referred to in this work as recycled magnets (RM). Interest in this particular particle size range was due to its previously seen high performance, yet poor mechanical properties around the edges of a flash SPS deformed sample [17]. The application of dies to control the deformation at the edges of the sample in both flash SPS and FAST/SPS deformation may lead to a more stable final magnet.

Characterization of magnet powders and microstructural characterization

Particle morphology and microstructures of the powders were analyzed via field emission gun scanning electron microscopy (FEG-SEM, referred to in this work as SEM) via SEM type Zeiss Gemini 450 (Carl Zeiss AG, Germany) using an acceleration voltage of 8 kV and working distance of 8.5 mm. A classical Everhardt-Thornley secondary electron (SE) detector was used for low magnifications,

and an InLens – SE detector was used for high magnifications. For material contrast images in which the phase distribution can be determined, a back scattered electron (BSE) detector was utilized. Oxygen contamination was analyzed using a NOH-analyzer type TCH 600 (LECO Corporation, USA).

Pre-sintering

For FAST/SPS deformation, 15 g of magnet powder was pre-compacted into a graphite die (SGL Carbon, SIGRAFINE R7710) with an inner diameter of 20 mm. For tool preservation and improvement of sample contact, a graphite foil with thickness 0.35 mm (SGL Carbon, SIGRAFLEX) was used to line the circumference of the die. FAST/SPS was performed in an HP-D5 device (FCT Systeme GmbH, Rauenstein, Germany), and all experiments were performed under a mild vacuum (< 1 mbar). The pellets were heated to a maximum temperature of 725 °C with a heating rate of 75 K min^{-1} and a dwell time at maximum temperature of 120 seconds. A constant pressure of 50 MPa (16 kN) was applied throughout the procedure. These pre-sintering parameters were chosen to produce near-dense pellets for deformation via FAST/SPS and were developed in collaboration with the work of Fraunhofer-Einrichtung für Wertstoffkreisläufe und Ressourcenstrategie (IWKS). Samples hot pressed using these parameters are labeled as “FAST-HP”.

For flash SPS deformation, 15 g of magnet powder was pre-compacted into the same type of graphite dies lined with the same foil as for the FAST/SPS pre-sintered pellets. However, temperature and dwell time differed from these preparations. For the flash SPS samples, FAST/SPS was performed in an HP-D5 device (FCT Systeme GmbH, Rauenstein, Germany), and all experiments were performed under mild vacuum (< 1 mbar). The pellets were heated to a maximum temperature of 500 °C with a heating rate of 100 K min^{-1} and a dwell time at maximum temperature of 60 seconds. A constant pressure of 50 MPa (16 kN) was applied throughout the procedure. These pre-sintering parameters were chosen due to their possibility of limiting grain growth prior to the flash SPS deformation step, as observed by Maccari *et al*.[16] Samples pre-sintered using these parameters are labeled as “FLASH-PS”.

Optimization of FAST/SPS deformation

FAST/SPS deformation experiments were performed in a hybrid FAST/SPS device (H-HP-D 25 SD/FL/MoSi from FCT Systeme GmbH, Rauenstein, Germany). 20 mm hot pressed pellets were placed inside a 30 mm titanium-zirconium-molybdenum (TZM) die which was likewise lined with graphite foil with thickness 0.35 mm (SGL Carbon, SIGRAFLEX). All experiments were performed under vacuum. The deformation followed a series of steps. First, samples were exposed to a pressure of 10 kN and heated at a rate of 100 K/min. Then, when the temperature reached 600 °C, the load was increased to 16 kN (50 MPa on a 20 mm sample), fully deforming the samples to fill the 30 mm diameter of the die. Heating continued at 100 K/min to the maximum temperature, 750 °C. At maximum temperature, pressure was increased for 1 minute to the target maximum pressure, ranging from 100-300 MPa. Pressure was released and cooling began once maximum pressure was achieved. Samples were then extracted and cut in half, with one half used for magnetic characterization by Permagraph C-300 system (MAGNET-PHYSIK Dr. Steingroever GmbH, Köln, Germany). The other half was preserved for microstructural characterization.

Optimization of flash SPS deformation with BN ring

Flash SPS experiments were performed in the same hybrid FAST/SPS device as the FAST/SPS deformation experiments, H-HP-D25. 20 mm pre-sintered pellets were placed inside boron nitride (BN) rings of diameters ranging from 25-30 mm. Experiments were performed under a vacuum of roughly 0.4 mbar. The samples that had been pre-sintered were placed between two graphite punches (diameter 60 mm) with plane parallel surfaces. A load of 10 kN (roughly 32 MPa for a 20 mm sample) was applied to the samples. The samples were then preheated to 600 °C via direct Joule heating with a maximum heating power of 15 kW. The samples then dwelled at maximum temperature for 120 s. After dwell, the samples were subjected to a pulse of continuous direct current at a maximum power of 35 kW for a duration of 30 s. At the end of the power pulse, the current was switched off to allow the sample to cool for 10 minutes before the vacuum was released and the chamber opened for sample extraction. Samples had edge and center pieces taken for magnetic characterization by Permagraph C-300 system (MAGNET-PHYSIK Dr. Steingroever GmbH, Köln, Germany).

Results and Discussion

MQU-F characterization

In Fig. 1, the MQU-F powder can be seen with its isotropic microstructure and flake-like morphology. The morphology helps attribute to the packed stacking of the powder during both the pre-sintering and deformation processes. As the microstructure is isotropic with equiaxed grains, the magnetic behavior is not yet optimal, as anisotropic grain growth and texture will need to be developed during deformation.

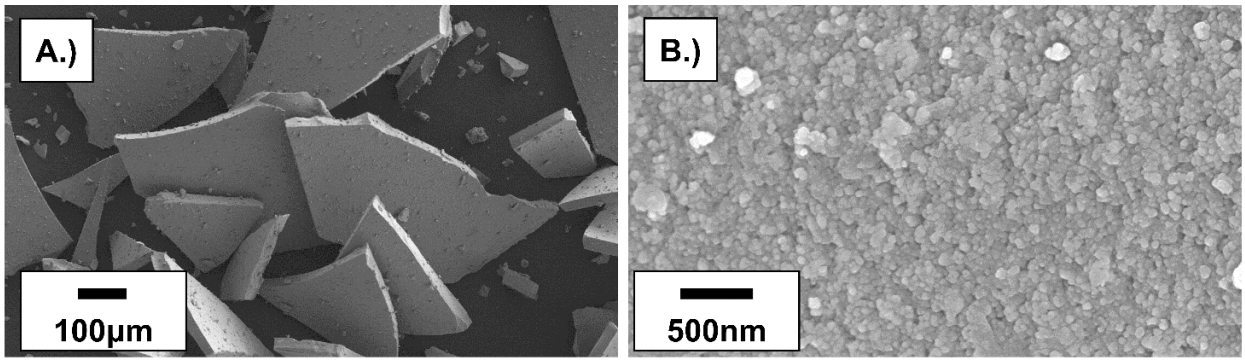

Fig. 1. SE SEM images of A.) MQU-F flakes and B.) their nanocrystalline isotropic microstructure

FAST/SPS deformation of MQU-F

FAST-HP samples were hot compacted in the FAST/SPS device to a density of roughly 93% (relative to 7.55 g/cm^3) and a height of approximately 7 mm. Photos of a pre-sintered sample in comparison to a deformed sample can be seen in Fig. 2. A rough surface topography appears during the deformation, which may be a result of the graphite foil shifting during the deformation. Nevertheless, magnet samples often have their faces polished so this is not of great concern. FAST-HP-P100T750, FAST-HP-P200T750, and FAST-HP-P300T750 are all samples deformed under pressures of 100, 200, and 300 MPa, respectively, at a maximum temperature of 750 °C. It was hypothesized that higher pressures would lead to better texturing of Nd-Fe-B and therefore higher remanence B_r. This, however, did not seem to be the case as all three samples deformed under various loads had similar remanence values, as can be seen in Table 1. The higher pressure seemed to be at a detriment of the coercivity for the samples, likely because it led to higher grain growth along the boundaries between different MQU-F flakes, as seen in Fig. 3. Here it is seen that, while all trials generated larger grain growth at the flake boundaries, the frequency increases when pressure increases from 100 to 200 MPa. FAST-HP-P300T750 also experiences grain growth beyond the contact points of MQU-F grains along with a higher frequency of large Nd-rich precipitations. These regions hinder magnetic performance through creating a larger decoupling effect between magnetic grains than is desired. FAST-HP-P100T750 has the best combination of remanence and coercivity relative to the other samples. This may be due to the pressure leading to good densification while not causing excessive grain growth. This is the case even though this sample had the lowest percentage change in height, despite the fact that high change in height is often seen as an indicator for optimal magnetic performance[26]. Anisotropic grain growth and texturing occurred in all deformation cases, as seen in Fig. 3, but the positive effects are hindered by abnormal grain growth appearing in all samples.

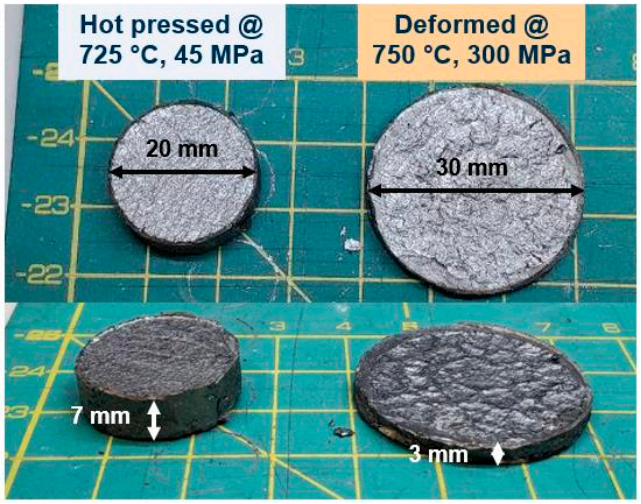

Fig. 2. FAST-HP hot pressed sample compared to a sample deformed by FAST/SPS

Table 1 – Magnetic behavior of the FAST-HP samples after FAST/SPS deformation

Sample Name	Remanence, B_r (T)	Coercivity, H_{cJ} (kA/m)	Energy Product, $(BH)_{max}$ (kJ/m^3)	Change in height (%)
FAST-HP-P100T750	1.17	1407	258	50
FAST-HP-P200T750	1.15	1279	242	53
FAST-HP-P300T750	1.18	1283	246	59

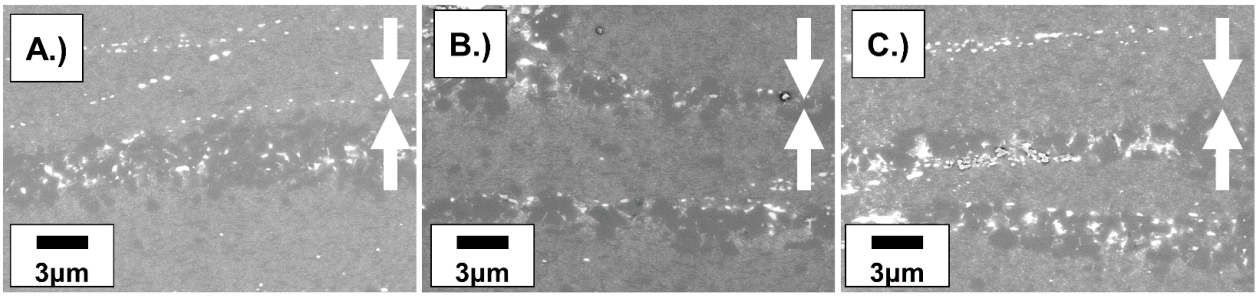

Fig. 3. – BSE SEM cross-section images of A.) FAST-HP-P100, B.) FAST-HP-P200, and C.) FAST-HP-P300. Dark grey in these images refer to the $Nd_2Fe_{14}B$ phase, while lighter grey is the Nd-rich grain boundary phase. Bright white zones are Nd-rich segregations. Deformation direction is denoted by white arrows.

Flash SPS deformation of MQU-F

Fig. 4 shows the FLASH-PS pre-sintered pellets after their deformation via flash SPS. Samples that were bound by the 30 and 29mm dies have clearly smoother and less cracked edges than their smaller die or no die counterparts. Despite the improved appearance of the magnets, magnetic performance was not simultaneously improved. A cylindric specimen with 2mm diameter was taken from the center of each sample, Table 2 shows how each magnet compares after deformation. The fragility of some samples, such as the one deformed with the 28mm die, did not allow for a sample to be taken for magnetic characterization. FLASH-PS-No-die still displays the best balance of coercivity and remanence compared to all other samples produced with dies. This may be due to the fact that the sample could fully deform without resistance, leading to a 68% change in height. FLASH-PS-30mm and FLASH-PS-29mm show similar behavior to one another, with the 30mm sample experiencing some detriment in remanence but no change in coercivity when compared to the 29mm sample. FLASH-PS-25mm seems to have hardly developed any anisotropic growth or texturing at all, as its remanence of 0.87 T is similar to that of an isotropic magnet. The constriction of the small 25mm die likely did not allow the deformation process to occur fully in this sample. As there was only one sample taken from this pellet for magnetic analysis, it may not be representative of the whole as deformation was still observed in this pellet.

In only two cases could both edge and center samples be taken for magnetic performance measurements. This was the case for FLASH-PS-No-die and FLASH-PS-30mm, as seen in Fig. 5. The use of a 30mm die certainly had an effect on the homogeneity of the magnetic performance from the edge to the center of the sample, as the hysteresis curves for edge and center overlap. FLASH-PS-No-die has a significant difference between the edge and the center, with the edge even appearing more improved than the sample center. This may be due to the center experiencing higher heat due to better contact with the electrodes, resulting in more grain growth. Edges also experience more material flow, which leads to higher anisotropy at sample edges. As seen in Fig. 6, some grains from the center of FLASH-PS-no-die extend beyond the desired 200-300nm width and reach widths of above 1µm. More striking is the fact that FLASH-PS-30mm contains grains with a size larger than 1µm in width and nearly 500nm in height. This growth is primarily seen in the contact regions between former MQU-F particles, much like in the FAST/SPS deformation case. It may be that this is seen more frequently in the FLASH-PS-30mm sample due to the constriction of the die. In the case of FLASH-PS-no-die, the Nd-Fe-B material is free to flow without bounds in two dimensions which allows mass transfer to occur outwards. In the case of FLASH-PS-30mm, restricted two-dimensional flow may cause buildup within the system, causing greater grain growth than in a sample where mass can flow.

Fig. 4. Photo of the samples deformed via flash SPS with and without boron nitride dies

Table 2 – Magnetic behavior of the FLASH-PS samples after flash SPS deformation (n.a. = not available)

Sample Name	Remanence, B_r (T)	Coercivity, H_{cJ} (kA/m)	Energy Product, $(BH)_{max}$ (kJ/m^3)	Change in height (%)
FLASH-PS-25mm	0.87	289	59	36
FLASH-PS-27mm	1.20	865	260	52
FLAHS-PS-28mm	n.a.	n.a.	n.a.	51
FLASH-PS-29mm	1.13	1346	235	54
FLASH-PS-30mm	1.09	1346	216	59
FLASH-PS-No-die	1.16	1321	236	68

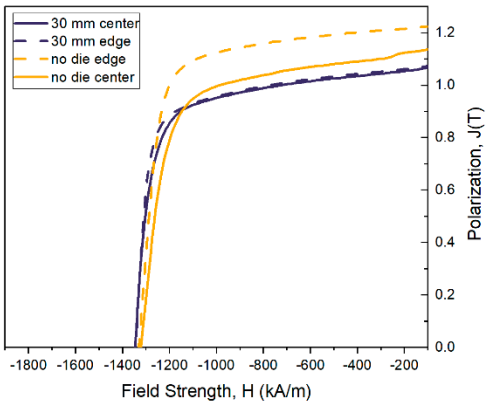

Fig. 5. Magnetic hysteresis curves (quadrant 2 only) of FLASH-PS-No-die and FLASH-PS-30mm with curves representing both edge and center measurements for both samples

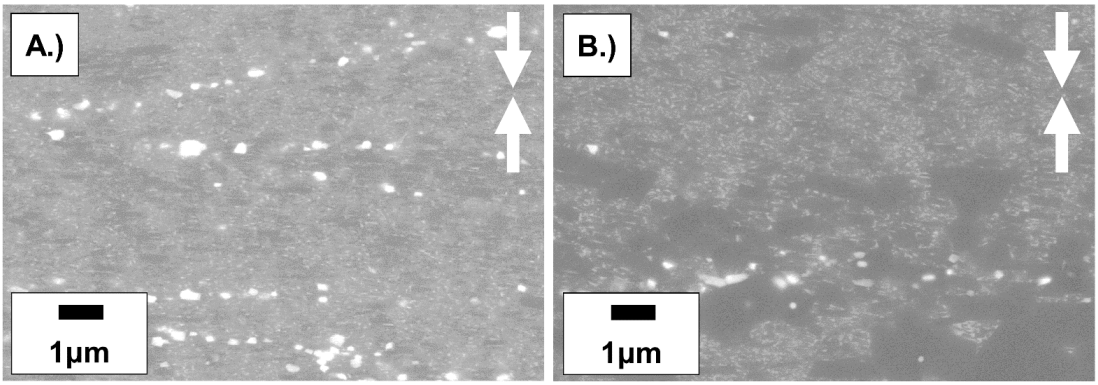

Fig. 6. BSE SEM cross-section images of the center region of A.) FLASH-PS-No-die and B.) FLASH-PS-30mm

Recycled material in deformation processes

At the time of writing, only one experiment has been performed on the RM powder. Pre-sintering for flash SPS samples and flash SPS deformation was done for one RM sample made from 100% scrap, resulting in the magnetic behavior listed in Table 3. This flash SPS deformation was performed without a BN ring, resulting in very cracked and mechanically weak edges on the sample, as seen in Fig. 7. This sub-optimal result is likely influenced by the powder being 500-1000 µm, which is unusually coarse for powder metallurgical processing. The excessive spread of the powder during deformation is partially what inspired the use of a BN ring in the production of flash SPS recycled magnets. Due to the unsatisfactory performance of MQU-F deformed in BN rings from 30-25 mm, however, deformation of RM in the BN rings has yet to be performed. Further information regarding samples mixed with this powder can be read about in our previous publication[17].

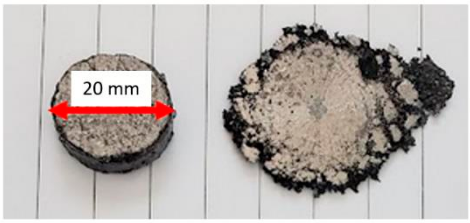

Fig. 7 – RM pellet after pre-sintering (left) and after flash SPS deformation (right) [17]

Table 3 – Magnetic behavior of the FLASH-PS-RM sample after flash SPS deformation

Sample Name	Remanence, B_r (T)	Coercivity, H_{cJ} (kA/m)	Energy Product, $(BH)_{max}$ (kJ/m^3)	Change in height (%)
FLASH-PS-RM-No-die	0.96	836	157	67

Some important observations in these preliminary trials with MQU-F have been made. Firstly, in the FAST-HP trials, it is likely that a hot pressing temperature of 725 °C will be detrimental to the incorporation of scrap anisotropic Nd-Fe-B. This is because this temperature is definitely inducing the melting phase of the grain boundary, even at the hot pressing step, which can result in excessive grain growth in the anisotropic scrap even before the deformation step [27]. A decrease in pre-sintering temperature will likely be necessary, even if it results in a compact that is not full dense prior to deformation. Secondly, the application of high pressures inducing large grains in the isotropic MQU-F will cause excessive grain growth in anisotropic scrap. Therefore, a new window of pressure parameters to be tested needs to be established. Even with the optimization of deformation using MQU-F, due to the already existing texture in recycled scrap, the behavior of recycled scrap to the same deformation parameters may vary greatly, which will need to be considered after optimization of processes with isotropic powder.

Conclusion

Both FAST/SPS and flash SPS deformation of MQU-F cause an anisotropic microstructure to develop. Excessive grain growth occurs in both cases at the meeting points of the MQU-F pristine flakes, though, leading to detriments in magnetic performance. High pressure (>100 MPa) accelerates this grain growth, likely due to increased mass transfer through the liquid grain boundary phase. With the application of a BN die in flash SPS deformation, too high constriction of the sample does not allow for anisotropic grain growth to develop. While the use of a die does seem to increase magnetic homogeneity and avoid cracked/frayed edges, samples produced without a die still outperform samples produced with a die.

Future experiments will focus on the following points:

1.) Finding an optimal pressure and temperature combination for FAST/SPS deformation

2.) Using larger BN dies (31-33 mm) to allow for full deformation of the pre-sintered pellet during flash SPS deformation

3.) Introducing recycled powder into the system and modifying optimized parameters to best fit the nature of the recycled scrap

Acknowledgements

This research was done in the framework of the project “EnerGieeffziENtE KreiSlaufwirtschaft krItischer RohStoffe (GENESIS)“, which is funded by the German Federal Ministry for Economic Affairs and Climate Action (BMWK) according to a decision of the German Federal Parliament. The funding is highly acknowledged. GENESIS is a joint project between the Ruhr-Universität Bochum, the Bergische Universität Wuppertal, the RWTH Aachen and the Forschungszentrum Jülich as scientific institutions, the German companies WILO SE, Klaus Kuhn Edelstahl, August Berghaus GmbH, Berger Gruppe as end users and Glamatronic, OWL and Dr. Fritsch Sondermaschinen GmbH as equipment manufacturers. Experimental support of Ralf Steinert (FAST/SPS) is greatly acknowledged.

References

1) Gutfleisch O., Willard, M. A., Brück E., Chen C. H., Sankar S. G., Liu J. P., *Adv. Mater.*, **23**, (2010).
2) Matsuura Y., *J. Magn. Magn. Mater.*, **303**, 344–347 (2006).
3) Sugimoto S., *J. Phys. Appl. Phys.*, **44**, (2011).
4) Kara H., Chapman A., Crichton T., Willis P., Morley N., Lanthanide Resources and Alternatives, Oakdene Hollins Research and Consulting, Aylesbury, United Kingdom, 2010.
5) Balaram V., *Geosci. Front.*, **10**, 1285–1303 (2019).
6) Yue M., Yin X., Liu W., Lu Q., *Chin. Phys. B*, **28**, 077506 (2019).
7) Mishra R. K., Brewer E. G., Lee R. W., *J. Appl. Phys.*, **63**, 3528–3530 (1988).
8) Yang Y., Walton A., Sheridan R., Güth K., Gauß R., Gutfleisch O., Buchert M., Steenari B.-M., Van Gerven T., Jones P. T., Binnemans K., *J. Sustain. Metall.*, **3**, 122–149 (2017).
9) Schönfeldt M., Rohrmann U., Schreyer P., Hasan M., Opelt K., Gassmann J., Weidenkaff A., Gutfleisch O., *J. Alloys Compd.*, **939**, 168709 (2023).
10) Diehl O., Schönfeldt M., Brouwer E., Dirks A., Rachut K., Gassmann J., Güth K., Buckow A., Gauß R., Stauber R., Gutfleisch O., *J. Sustain. Metall.*, **4**, 163–175 (2018).

11) Zakotnik M., Harris I. R., Williams A. J., *J. Alloys Compd.*, **469**, 314–321 (2009).
12) Habibzadeh A., Kucuker M. A., Gökelma M., *ACS Omega*, **8**, 17431–17445 (2023).
13) Hioki K., *Sci. Technol. Adv. Mater.*, **22**, 72–84 (2021).
14) Mishra R. K., *J. Appl. Phys.*, **62**, 967–971 (1987).
15) Une Y., Sagawa M., *J. Jpn. Inst. Met.*, **76**, 12–16 (2012).
16) Maccari F., Mishra T. P., Keszler M., Braun T., Adabifiroozjaei E., Radulov I., Jiang T., Bruder E., Guillon O., Molina-Luna L., Bram M., Gutfleisch O., *Adv. Eng. Mater.*, (2023).
17) Keszler M., Grosswendt F., Assmann A.-C., Krengel M., Maccari F., Gutfleisch O., Sebold D., Guillon O., Weber S., Bram M., *Adv. Energy Sustain. Res.*, **5**, 2300184 (2024).
18) Prasad Mishra T., Leich L., Krengel M., Weber S., Röttger A., Bram M., *Adv. Eng. Mater.*, **25**, 2201027 (2023).
19) Yang Y. F., Qian M., "Titanium Powder Metallurgy," Elsevier, 2015, pp.219–235.
20) Bocchini G. F., *Powder Metall.*, **26**, 101–113 (1983).
21) Mamedov V., *Powder Metall.*, **45**, 322–328 (2002).
22) Leich L., Röttger A., Kuchenbecker R., Theisen W., *J. Mater. Sci. Mater. Electron.*, **31**, 20431–20443 (2020).
23) Leich L., Röttger A., Theisen W., Krengel M., *J. Magn. Magn. Mater.*, **460**, 454–460 (2018).
24) Leich L., Röttger A., Krengel M., Theisen W., *J. Sustain. Metall.*, **5**, 107–117 (2019).
25) Li X., Yue M., Zakotnik M., Liu W., Zhang D., Zuo T., *J. Rare Earths*, **33**, 736–739 (2015).
26) Grünberger W., Hinz D., Kirchner A., Müller K.-H., Schultz L., *J. Alloys Compd.*, **257**, 293–301 (1997).
27) Grieb B., Henig E.-Th., Schneider G., Knoch G., Petzow G., de Mooij D., *Powder Metall.*, **35**, 221–229 (1992).

Received June 10, 2024; Revised August 26, 2024; Accepted September 9, 2024